THE JOURNAL OF PHYSICAL CHEMISTRY C
A JOURNAL OF THE AMERICAN CHEMICAL SOCIETY

pubs.acs.org/JPCC

Article

Correct and Accurate Polymorphic Energy Ordering of Transition-Metal Monoxides Obtained from Semilocal and Onsite-Hybrid Exchange-Correlation Approximations

Arghya Ghosh, Subrata Jana,* Manish K. Niranjan, Fabien Tran, David Wimberger, Peter Blaha, Lucian A. Constantin, and Prasanjit Samal

Cite This: *J. Phys. Chem. C* 2022, 126, 14650−14660

Read Online

ACCESS | Metrics & More | Article Recommendations | Supporting Information

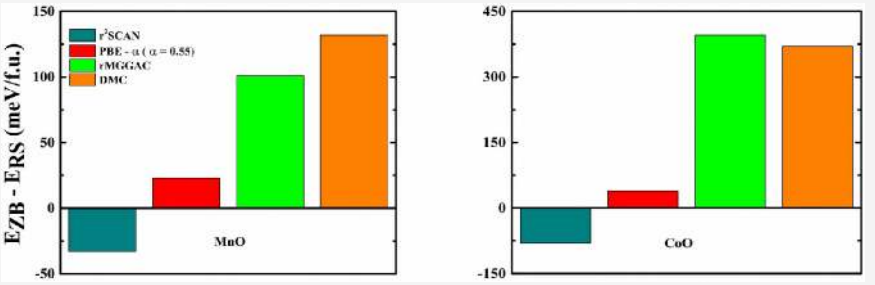

ABSTRACT: The relative energetic stability of the structural phases of common antiferromagnetic transition-metal oxides (MnO, FeO, CoO, and NiO) within the semilocal and hybrid density functionals are fraught with difficulties. In particular, MnO is known to be the most difficult case for almost all common semilocal and hybrid density approximations. Here, we show that the meta-generalized gradient approximation (meta-GGA) constructed from the cuspless hydrogen model and Pauli kinetic energy density (MGGAC) can lead to the correct phase as the ground-state of MnO. The relative energy differences of zinc blende (*zb*) and rock salt (*rs*) structures as computed using MGGAC are found to be in nice agreement with those obtained from high-level correlation methods like the random phase approximation or quantum Monte Carlo techniques. Besides, we have also applied the onsite hybrid functionals (closely related to DFT+*U*) based on GGA and meta-GGA functionals, and it is shown that a relatively high amount of Hartree−Fock exchange is necessary to obtain *rs* as the ground-state phase. Our present investigation suggests the semilocal MGGAC and onsite hybrids, both being computationally cheap, as methods of choice for the calculation of the relative stability of antiferromagnetic transition-metal oxides having potential applications in solid-state physics and structural chemistry.

INTRODUCTION

The Kohn−Sham (KS) density functional theory (DFT)[1,2] has become a highly successful and indispensable tool for studying the structural and electronic properties of condensed matter systems.[3−5] However, the accuracy and reliability of DFT depend crucially on the various approximations for the exchange-correlation (XC) energy functional,[6] which includes all the many-body effects beyond the Hartree approximation. During the last few decades, several accurate approximations for the semilocal XC functionals, which are the computationally cheapest methods in DFT, have been proposed. However, their application to transition-metal oxides (TMOs) compounds having open *d*-shell still remains challenging[7−14]

Here, we revisit the relative accuracy of different levels of XC methods to predict the ground-state properties of a prototypical open *d*-shell TMO, namely MnO, which is potentially very interesting in industrial applications, for example, photoelectrochemical water splitting,[15,16] solar energy conversion,[17] or magneto-piezoelectric effect.[18] A large number of theoretical studies have been carried out for MnO phases[8−11,19,20] that have led to the identification of different polymorphic phases:[9] rock salt (*rs*), zinc blende (*zb*), and wurtzite (*wz*). Concerning magnetism, MnO is antiferromagnetic (AF) with ferromagnetic planes stacked along the [111] (AF2) and [001] (AF1) directions for the *rs* and *zb* structures, respectively. Among the phases *rs*-AF2 and *zb*-AF1, the first one is found as the most stable one according to the experiment,[21] as well as the random phase approximation (RPA)[8] and Diffusion Monte Carlo (DMC) methods,[10] which are high-level ab initio methods. However, this is not the case with the common generalized gradient approximations (GGA) and hybrid DFT XC methods that incorrectly predict the

Received: May 20, 2022
Revised: August 4, 2022
Published: August 19, 2022

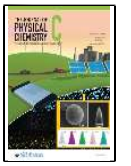

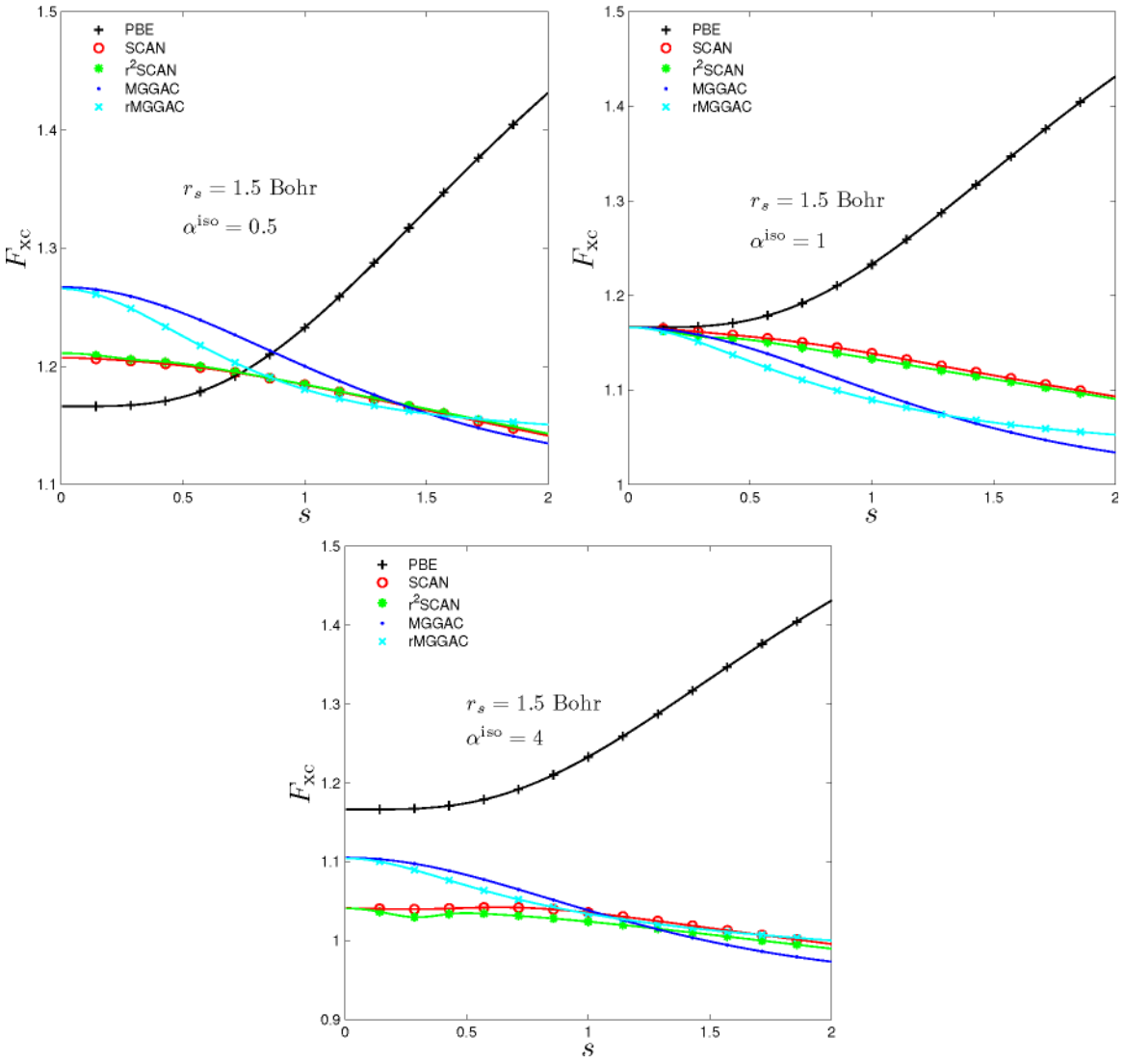

Figure 1. Enhancement factors F_{XC} plotted as a function of s. The values of r_s and α^{iso} (that are kept fixed) are indicated in the respective panels. Note the different scales on the vertical axis.

energy of the *zb*-AF1 phase to be lower than that of *rs*-AF2.[8−11,22] However, GGA+*U* (GGA with a Hubbard *U* correction) predicts the correct ground state of MnO, although a large and unphysical *U* value is required.[15]

One may note that in addition to the aforementioned works, a very large number of other studies have investigated the ground-state or electronic properties of the *rs*-AF2 phase of MnO. A certain number of DFT and beyond DFT methods are used, and this includes many semilocal DFT methods (see refs 11 and 23−26 for recent work), DFT+*U*,[27,28] various types of hybrids,[29−35] the self-interaction corrected local density approximation,[7] the optimized effective potential method,[36,37] model Hamiltonian approach,[19,38−40] the quasi-particle GW method,[41−43] and dynamical mean field theory (DMFT).[44−46] Nevertheless, it is important to mention that the most accurate of all these methods, namely, RPA, DMC, GW, and DMFT are computationally much more expensive than DFT-based methods.

Hence, from the point of view of efficiency, the preferred methods are the semilocal XC functionals in DFT. In particular, we mention that SCAN+rVV10+*U*, which consists of the strongly constrained and appropriately normed (SCAN) meta-GGA[47] combined with the rVV10 van der Waals (vdW)[48] functional and a Hubbard *U* correction, has been found to perform well in case of TMOs.[11] It is clearly admitted that the meta-GGA functionals generally perform better than the GGAs in describing solid-state properties.[47,49−54] Concerning MnO, it has been shown that the polymorphic structural energy difference computed using SCAN+rVV10+*U*, where *U* is determined from linear response theory, agrees very well with that obtained from DMC values.[11] Besides the SCAN-based methods, several other meta-GGA functionals are also proposed and tested for solid-state properties with consistently improved accuracy.[49,54−65] Within those recent meta-GGAs, there are the functionals constructed from the cuspless hydrogen model [(revised) meta-GGA functional from cuspless hydrogen hole ((r)MGGAC)][62,65] that show potential promising accuracy for different challenging problems in solid-state physics.[54,64,65] It is also quite an efficient semilocal functional that can predict band gaps of bulk and layered solids with reasonable accuracy.[54,65−68]

Inspired by the promising performance of the (r)MGGAC functionals for solids, in the present paper we investigate the polymorphic energy ordering of MnO, FeO, CoO, and NiO

https://doi.org/10.1021/acs.jpcc.2c03517
J. Phys. Chem. C 2022, 126, 14650−14660

using these methods, with a particular focus on MnO. Our results will also be compared with those obtained from other DFT methods and higher-level quantum methods.

Among the other DFT methods, we chose the onsite hybrids[29,69] that consist of a simplification of the well-known hybrids, where the Hartree−Fock exchange is applied only inside the atomic region surrouding the transition-metal atom.

This paper is organized as follows. In Theoretical Background we first briefly describe the methods that we used for the calculations. Next, the computational setup of the present calculations is given in Computational Details. Then, in Results we present and discuss the results obtained for the polymorphic energy ordering of different TMOs, and the conclusions are presented in Conclusions.

THEORETICAL BACKGROUND

Belonging to the semilocal levels of approximation, the functionals PBE,[70] SCAN,[47] r^{2}SCAN,[71] MGGAC,[62] and rMGGAC[65] are considered for our calculations. Details about the functionals can be found in the correponding works. Here, we only briefly discuss about the meta-GGAs (r^2)SCAN and (r)MGGAC. Meta-GGA functionals can be written as ($n = \sum_i |\psi_i|^2$ and $\tau = (1/2)\sum_i \nabla\psi_i^* \cdot \nabla\psi_i$, where $\sum_i$ sums are over occupied orbitals, i.)

$$E_{XC} = \int \epsilon_{XC}(n, \nabla n, \tau) d^3r = \int \epsilon_X^{LDA}(n) F_{XC}(r_s, s, \alpha^{iso}, z) d^3r \quad (1)$$

where $\epsilon_X^{LDA} = -(3/4)(3/\pi)^{1/3} n^{4/3}$ is the exchange-energy density of the local density approximation (LDA) and F_{XC} is the XC enhancement factor. The n, ∇n, and τ dependencies of F_{XC} are usually expressed via the Wigner-Seitz radius $r_s = (3/(4\pi n))^{1/3}$, the reduced density gradient $s = |\nabla n|/(2(3\pi^2)^{1/3} n^{4/3})$, and the iso-orbital indicators $\alpha^{iso} = (\tau - \tau^W)/\tau^{UEG}$ and $z = \tau^W/\tau$, where τ^W and τ^{UEG} are the von Weizsäcker and uniform electron gas (UEG) kinetic-energy densities. Noteworthy, α^{iso} recognizes regions with single bonds, overlapping orbitals, and uniform density.[72,73] Note that $F_X^{(r^2)SCAN}$ depends on both s and α^{iso}, while $F_X^{(r)MGGAC}$ depends only on α^{iso}. But none of these functionals depends on $z;\lambda$ therefore they are free from the order-of-limit problems.[50,74] Whereas, functionals like Tao-Perdew-Staroverov-Scuseria (TPSS)[75] and Tao-Mo[76] depend on s, α^{iso}, and z and suffer from order-of-limit problems.[77] These functionals are generally not considered for structural phase stabilities, which are the main focus of the present paper.

In brief, the SCAN functional was constructed such that it satisfies 17 exact mathematical constraints that can be satisfied by a meta-GGA. For instance, the exchange component of the xc enhancement factor, F_X^{SCAN}, recovers the exact fourth-order gradient approximation of exchange. r^{2}SCAN is a slightly modified version of SCAN that alleviates numerical problems encountered with SCAN. The development of the MGGAC functional is rather unusual and unconventional. The exchange part is based on the Becke-Roussel approach[78] and with a cuspless hydrogen exchange hole density.[79] MGGAC differs from SCAN for the following two reasons. First, only the exchange component of MGGAC is a meta-GGA, while the correlation part is a GGA. Second, F_X^{MGGAC} depends only on α^{iso} (and not on s). However, the correlation part of rMGGAC is of the meta-GGA type.[65] It is worth mentioning that (r^2)SCAN and (r)MGGAC respect the strongly tightened bound exchange ($F_X \leq 1.174$[47,80]) and possess ultranonlocality effects, which is important for the band gap problem.[62,66,81] It may also be noted that MGGAC correlation is not free from the one-electron self-interaction error, whereas rMGGAC is.

Figure 1 compares the PBE, (r^2)SCAN, and (r)MGGAC enhancement factors F_{XC}. This will be useful to understand the results discussed later in this work. An obvious difference between the GGA PBE and the meta-GGAs concerns the sign of $\partial F_{XC}/\partial s$. While $\partial F_{XC}/\partial s$ is positive for PBE, it is negative for all four meta-GGAs. One may note that in general the slope $\partial F_{XC}/\partial s$ of meta-GGAs can be positive or negative depending on the particular meta-GGA, but also, to a lesser extent, on the chosen fixed values of r_s or α^{iso} (see ref 26 for plots of F_{XC} for other meta-GGAs). The other difference between PBE and the meta-GGAs concerns of course the variation with respect to α^{iso}. Since PBE is a GGA, $\partial F_{XC}/\partial\alpha^{iso} = 0$. The meta-GGAs have a negative value of $\partial F_{XC}/\partial\alpha^{iso}$ as for most meta-GGAs.[26] As discussed in ref 81, a more negative slope $\partial F_{XC}/\partial\alpha^{iso}$ leads to a larger derivative discontinuity, and consequently also to a larger band gap.[62,66]

Also considered in this work are the onsite hybrid functionals PBE-α and SCAN-α. They share close similarities with the DFT+U method, in particular since they are also applied only to the strongly correlated electrons, while the rest of the electrons are treated at the semilocal level.[29,69] Three different values of the amount of Hartree−Fock exchange α (0.25, 0.40, and 0.55) are used. Note that in the SCAN-α calculations, the functional derivative of the meta-GGA SCAN is replaced by the PBE potential. The reason is that a self-consistent implementation of SCAN when combined with onsite Hartree−Fock exchange is not yet available. However, this should have a relatively small influence on the results for the geometry and relative phase stability, in particular since the main effect is due to the Hartree−Fock exchange, which is applied self-consistently.

Regarding the computational cost of the considered functionals, meta-GGA functionals are only slightly more expensive than GGA functionals. The cost for evaluating the onsite Hartree−Fock exchange is relatively modest, which makes onsite hybrids by far much cheaper than the real hybrids that we have not consisdered in the present work.

Let us mention that within DFT, a formally more correct alternative to the "Hartree-Fock exchange" term would be "single-determinant exchange". However, we prefer to keep "Hartree-Fock since it is the standard along with "exact exchange".

COMPUTATIONAL DETAILS

The calculations on the TMOs MnO, FeO, CoO, and NiO with the r^{2}SCAN and (r)MGGAC meta-GGA functionals were performed using the Vienna Ab initio Simulation Package (VASP, version 5.4.4) code,[82−85] which is based on the projector augmented wave method.[85,86] The used PAW data sets are the standard ones and correspond to the valence electron configurations $3d^6 4s^1$ for Mn, $3d^7 4s^1$ for Fe, $3d^8 4s^1$ for Co, $3d^9 4s^1$ for Ni, and $2s^2 p^4$ for O. A plane-wave energy cutoff of 520 eV was used and the Brillouin zone was sampled using Monkhorst−Pack k-points grids that are approximately equivalent to 12 × 12 × 12 and 13 × 13 × 9 for four-atom rs and zb cells, respectively. The self-consistent field convergence was achieved with a criterion of 10^{-6} eV for the total energy.

The calculations with the onsite hybrid functionals were done using the all-electron WIEN2k code,[87,88] which is based

https://doi.org/10.1021/acs.jpcc.2c03517
J. Phys. Chem. C 2022, 126, 14650−14660

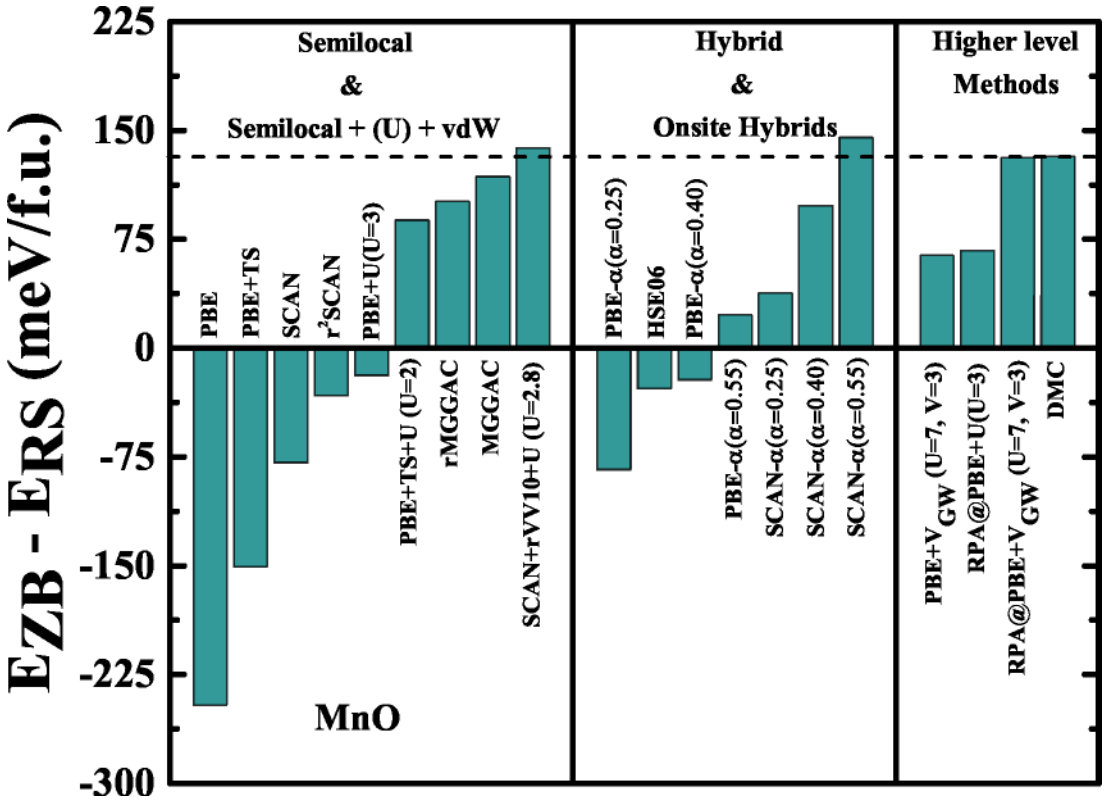

Figure 2. Total energy difference $\Delta E = E_{zb}^{AF1} - E_{rs}^{AF2}$ (in meV/f.u.) between the *zb*-AF1 and *rs*-AF2 phases of MnO. A positive energy difference indicates that *rs*-AF2 is energetically more stable than *zb*-AF1 (as experimentally determined). The MGGAC, rMGGAC, r^{2}SCAN, and onsite hybrids results are calculated for this work. The results obtained with the other methods are from refs 11 (PBE, PBE+TS, PBE+*U*, PBE+TS+*U*, SCAN+rVV10+U, and HSE06), 8 (the higher level methods except DMC), and 10 (DMC). See Table S2 for the details of the reference data used in this plot.

on the augmented plane-wave plus local orbitals method.[89,90] A value of at least $R_{MT}^{min}K_{max} = 8$ (the product of the smallest of the atomic sphere radii R_{MT} and the plane wave cutoff parameter K_{max}) was used for the expansion of the basis set. k-points grids similar to the ones mentioned above for the VASP calculations were used.

Regarding the phases of the TMOs, we will consider the *rs* and *zb* structures with the magnetic arrangements AF2 and AF1, respectively (see Figure S1 of the Supporting Information[91]). Calculations on the *wz*-AF1 phase (see Figure S2 and Table S1 of the Supporting Information[91]) were also done and will be briefly mentioned.

The ground-state properties (equilibrium volume and isothermal bulk modulus) were determined by performing a fit of the total energy versus volume with the third order Birch−Murnaghan isothermal equation of state.[92]

RESULTS

The calculated total energy difference $\Delta E = E_{zb}^{AF1} - E_{rs}^{AF2}$ and stability of the *zb*-AF1 phase relative to the experimentally determined ground-state *rs*-AF2 phase of MnO are shown graphically in Figure 2, while the numerical values can be found in Table S2 of the Supporting Information.[91] The results obtained with PBE, (r^2)SCAN, (r)MGGAC, and the onsite hybrids were obtained for the present work and are compared to results from the literature obtained with other methods. As mentioned in introduction, methods from various levels of theory, including semilocal, vdW-corrected, and high-level correlation methods, have been used and proposed in previous works to correctly describe the relative phase stability of MnO and to provide estimates of ΔE. In the present work, we consider the DMC value ΔE^{DMC} = 132 meV/f.u. from ref 10 as the reference benchmark. One may note that all calculations done for the present work, as well as those taken from the literature are for T = 0 K.

We mention again that RPA correctly leads to *rs*-AF2 as the ground-state phase.[8] Compared to DMC, the value ΔE = 67 meV/f.u. from RPA@PBE+U (U = 3 eV) (PBE+U orbitals used as input to RPA) is too small by a factor of 2, while ΔE = 131 meV/f.u from RPA@PBE+V_{GW} (U = 7 eV and V = 3 eV) matches perfectly the DMC value (in PBE+V_{GW} a nonlocal external potential V_{GW} on Mn *d* orbitals is used on top of the onsite U). In ref 11 it is shown that the correct phase ordering can also be obtained by adding vdW (Tkatchenko-Scheffler (TS)[93] or rVV10[94]) and Hubbard U (obtained from linear-response approach) corrections to a semilocal functional. The proposed PBE+TS+U (U = 3.2 eV)[11] and SCAN+*r*VV10+U (U = 2.8 eV)[11] lead to ΔE = 88 and 138 meV/f.u., respectively, the latter value agreeing very well with DMC.

However, as clearly visible in Figure 2, there are also a certain number of other popular methods that fail in predicting *rs* as the ground-state phase of MnO. Besides plain PBE, it is also the case with PBE+U with a small value of U (3 eV), the hybrid functional HSE06, and PBE+TS.[8] The meta-GGAs (r^2)SCAN also lead to the wrong phase for the ground state, however, the two other meta-GGAs tested in this work, MGGAC and rMGGAC, lead to positive energy differences, indicating that *rs*-AF2 is more stable than *zb*-AF1. Thus,

https://doi.org/10.1021/acs.jpcc.2c03517
J. Phys. Chem. C 2022, 126, 14650−14660

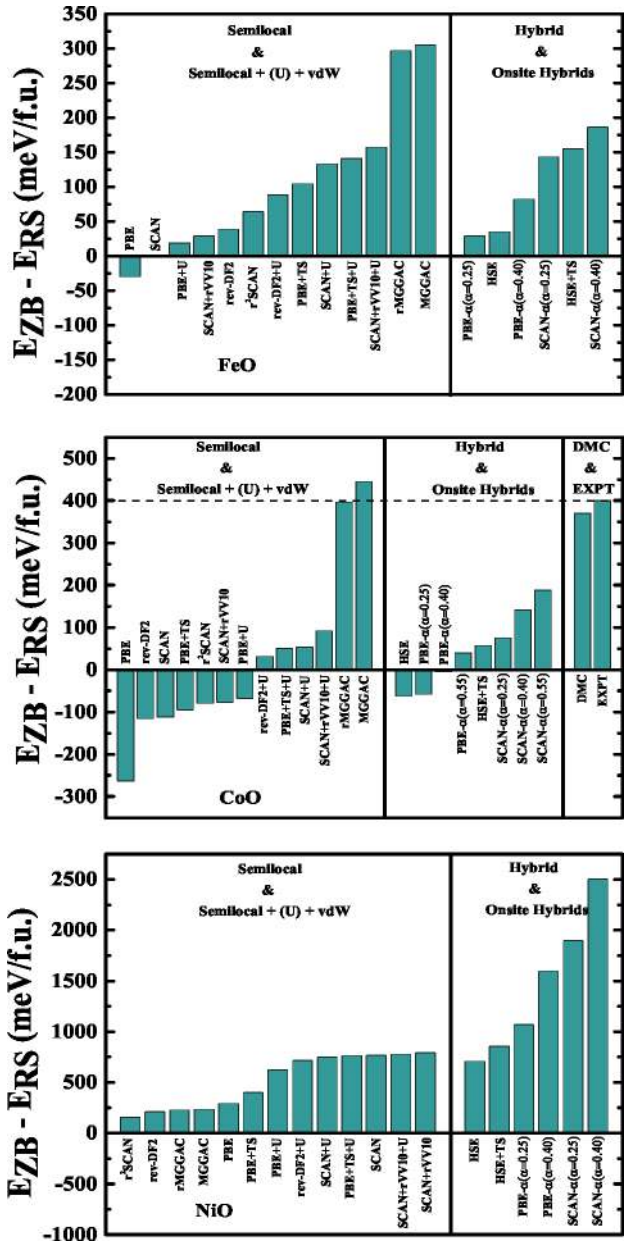

Figure 3. Total energy difference $\Delta E = E_{zb}^{AF1} - E_{rs}^{AF2}$ (in meV/f.u.) between the *zb*-AF1 and *rs*-AF2 phases of FeO (upper panel), CoO (middle panel), and NiO (lower panel). A positive energy difference indicates that *rs*-AF2 is energetically more stable than *zb*-AF1. The MGGAC, rMGGAC, r^{2}SCAN, and onsite hybrids results are calculated for this work. The results obtained with the other methods are from refs 11 (all DFT methods) and 10 (DMC).

MGGAC and rMGGAC are successful in predicting correctly the polymorphic energy ordering of the MnO phases. These are very interesting results, in particular when considering that no Hubbard *U* or vdW corrections are added to (r)MGGAC. Actually, as evident from the results, MGGAC and rMGGAC give the best performance among the semilocal methods. They lead to values for ΔE of 118 and 101 meV/f.u., respectively, which agree quite well with the reference value 132 meV/f.u. from DMC.

Regarding the performance of the onsite hybrids PBE-α and SCAN-α, also tested for the present work, we can see that the energetic ordering of the *rs*-AF2 and *zb*-AF1 phases depends

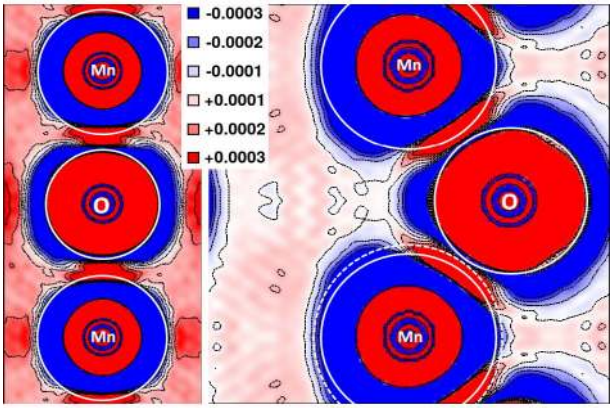

Figure 4. Two-dimensional plot in MnO of the difference (in Ry/Bohr^3) $\epsilon_{XC}^{SCAN} - \epsilon_{XC}^{MGGAC}$ between the SCAN and MGGAC XC energy density (see eq 1) obtained with WIEN2k from nonself-consistent calculations using the PBE electron density. The left and right panels show the (110) plane of *rs*-AF2 and the (001) plane of *zb*-AF1, respectively. The blue and red regions correspond to negative and positive values, respectively. The solid white circles show the atomic sphere of the Mn (1.98 Bohr) and O (1.71 Bohr) atoms, while the dashed white circle shows an enlarged atomic sphere (2.10 Bohr, see discussion in text) of the Mn atoms.

on the amount of the Hartree−Fock exchange α. For a correct energetic ordering, PBE-α requires a value of α larger than 0.40, which is quite high and clearly larger than the standard value $\alpha = 0.25$. For SCAN-α, $\alpha = 0.25$ is already sufficient. We can also see that the more α is large, the more the energetic ordering will go in the right direction. This is in agreement with the results from Schiller et al.[10] who considered hybrid functionals based on PBE (however, they found that *rs*-AF2 becomes more stable already at $\alpha = 0.10$). This behavior is also similar to what is obtained with DFT+*U*, with *U* playing the same role as α.[8,15]

The (r^2)SCAN and (r)MGGAC results discussed so far are obtained self-consistently using the VASP code.[82−85] It may be of interest to determine how important is self-consistency for the results, in particular in the case of (r)MGGAC, which lead to very good results. It is generally believed that in most cases self-consistency plays only a minor role and that using for instance the PBE electron density and orbitals (instead of those from (r)MGGAC) would not affect much the total energy computed with the (r)MGGAC energy functional. However, it may not be always the case, as discussed in ref.[101] for the closely related density-driven error. To make this point more clear for the results in the present work, we also calculated ΔE for (r)MGGAC and (r^2)SCAN using the PBE orbitals and electron density. These non-self-consistent calculations are performed using the all-electron code WIEN2k and the results are reported in Table 1. We can see that by using the PBE density and orbitals the trends do not change, that is, the ordering of the phases with (r)MGGAC is still correct, whereas it is not the case with (r^2)SCAN. There are some differences between the VASP self-consistent and WIEN2k nonself-consistent results, however they are unimportant for the conclusion. Overall, this indicates that the effect is essentially functional-driven.

Next, we consider in detail the results for the structural, electronic, and magnetic properties of *rs*-AF2MnO, calculated with the semilocal and onsite hybrid functionals. Our results are summarized in Table 2 and are compared to experimental

https://doi.org/10.1021/acs.jpcc.2c03517
J. Phys. Chem. C 2022, 126, 14650−14660

Table 1. Total Energy Difference $\Delta E = E_{zb}^{AF1} - E_{rs}^{AF2}$ (in meV/f.u.) between the *zb*-AF1 and *rs*-AF2 Phases of MnO Obtained Non-Self-Consistently with Different Functionals Using the PBE Orbitals and Electron Density[a]

	PBE	SCAN@PBE	r^{2}SCAN@PBE	MGGAC@PBE	rMGGAC@PBE
ΔE	−243	−87	−57	109	84

[a]The calculations are performed using the all-electron code WIEN2k.

Table 2. Lattice Constant a_0, Bulk Modulus B_0, Band Gap E_g, and Magnetic Moment μ of the Mn Atom of the *rs*-AF2 Phase of MnO Obtained from Different Methods[a]

method	a_0 (Å)	B_0 (GPa)	E_g (eV)	μ (μ_B)
PBE	4.438	149	0.72	4.38
SCAN	4.411	163	1.47	4.49
r^{2}SCAN	4.418	166	1.52	4.50
MGGAC	4.381	185	1.77	4.52
rMGGAC	4.392	178	1.70	4.52
PBE-α (α = 0.25)	4.488	144	1.21	4.65
SCAN-α (α = 0.25)	4.447	161		
PBE-α (α = 0.40)	4.512	141	1.34	4.74
SCAN-α (α = 0.40)	4.465	158		
PBE-α (α = 0.55)	4.531	139	1.45	4.80
SCAN-α (α = 0.55)	4.482	156		
expt[9]	4.4365,[b] 4.4315,[c] 4.4302[d]	149.6,[e] 146.7,[f] 148/144[g]	3.6−3.8[h]	4.58[c]

[a]The calculations with the PBE, SCAN, r^{2}SCAN, MGGAC, and rMGGAC are performed self-consistently using the VASP code. In WIEN2k code the PBE-α calculations are performed self-consistently. But the SCAN functional in SCAN-α was applied non-self-consistently using PBE-α densities and orbitals. Since the SCAN-α calculations are done non-self-consistently using PBE potential, the values of E_g and μ are omitted. [b]T = 4.2 K. Ref 95. [c]T = 5 K. Ref 96. [d]T = 8 K. Ref 97. [e]Ref 98. [f]Ref 99. [g]Ref 100. [h]See Table 1 of ref 10.

results (see ref 9). The experimental equilibrium lattice constant $a_0 \sim 4.43$ Å is best reproduced by PBE. (r^2)SCAN and SCAN-α (α = 0.25) are also pretty accurate. For the bulk modulus B_0, PBE is again the best method, and PBE-α can be also very accurate depending on the value of α. (r)MGGAC are not so accurate since they underestimate a_0 by 0.04−0.05 Å, while B_0 is too large by about 30 GPa.

The experimental band gap of 3.6−3.8 eV is strongly underestimated by at least 2 eV by all methods in Table 2. In a recent study[25] it was shown that among the fast semilocal DFT methods only the GLLB-SC[102] and Sloc[103] functionals are able to give band gaps of MnO similar to experiment. Other studies[10,43] have shown that GW can be accurate depending on the input orbitals, while DMC gives a band gap that is too large by nearly 1 eV.[10] The magnetic moment μ on the Mn atom was calculated inside the atomic basin as defined by the quantum theory of atoms in molecules of Bader.[104,105] The experimental value of 4.58 μ_B is best reproduced by the MGGAC, rMGGAC, and PBE-α (α = 0.25) functionals that give 4.52, 4.52, and 4.65 μ_B, respectively. However, using a larger value of α for the onsite hybrids leads to a clear overestimation of μ, as shown in Table 2.

Finally, we show in Figure 3 the results for the other antiferromagnetic TMOs considered in this work: FeO, CoO, and NiO. As for MnO, their ground-state phase is *rs*-AF2,[21] and we can see that this is correctly predicted by the MGGAC and rMGGAC functionals.

Neither experimental data nor values obtained from highly accurate methods like DMC or RPA seem to be available for FeO. Therefore, a comparison of the values of ΔE can be made only between DFT methods. As in the cases of MnO and CoO (see below), (r)MGGAC lead to the largest positive values of ΔE, too. They are clearly larger than for all other methods. Next come the onsite hybrid SCAN-α and *U*- and/or vdW-corrected functionals like SCAN+rVV10+*U* or rev-DF2+*U*.[11,106] Only PBE and SCAN lead erroneously to *zb*-AF1 as the ground-state phase, while a small amount of Hartree−Fock exchange α or small value of *U* is enough to get the correct ground-state phase *rs*-AF2.

For CoO, the experimental and DMC values (see ref 107 and references therein) of energy difference, $\Delta E = E_{zb}^{AF1} - E_{rs}^{AF2}$ are around 400 meV/f.u. and are reproduced very accurately by (r)MGGAC, as visible on Figure 3. Considering the onsite hybrid functionals based on SCAN, using larger values of α leads to better agreement with experiment and DMC, however the values are twice too small even with α = 0.55. Values from the literature[8,10,11,107] obtained with other methods are also shown in Figure 3. As for MnO, the popular methods PBE, SCAN, and HSE06 fail since they predict *zb*-AF1 to be more stable than *rs*-AF2, but adding a Hubbard *U* and/or vdW correction helps to get the correct trend.

As for FeO, no reference data is available for NiO. By inspecting the DFT results, we can see that the situation is quite different compared to MnO, FeO, and CoO. First, all functionals, without exception, lead to *rs*-AF2 as the ground-state phase. Second, the MGGAC and rMGGAC values are basically the smallest in magnitude, while the reverse was obtained for MnO, FeO, and CoO. The largest values of ΔE are obtained with the onsite hybrids SCAN-α and PBE-α. They are much larger than what is obtained with the other methods, and similar to the experimental formation enthalpy (2.5 eV/f.u.[108]), indicating that the metallic *zb* phase is quite unfavorable. Actually, this is not too surprising considering the fact that the e_g-t_{2g} crystal-field splitting is reversed in *zb*, so that the three minority-spin 3*d* electrons have to fill first the two e_g states and then one of the three high-lying t_{2g} states.

In order to show that the (r)MGGAC functionals lead to the correct energy ordering also for other phases of the studied systems, we considered the *wz*-AF1 phase.[9] The values of $\Delta E^{wz-rs} = E_{wz}^{AF1} - E_{rs}^{AF2}$ are presented in Tables S3 and S4 of ref

https://doi.org/10.1021/acs.jpcc.2c03517
J. Phys. Chem. C 2022, 126, 14650−14660

91. For the four systems the (r)MGGAC values of ΔE^{wz-rs} are positive, which is the correct trend. Reference (experimental and DMC) values for ΔE^{wz-rs} are available only for CoO,[107] and we can see that the magnitude of ΔE^{wz-rs} obtained with (r)MGGAC is too large by roughly ∼200 meV/f.u. compared to the reference values.

At this point one may wonder why the (r)MGGAC functionals work much better than PBE and (r^2)SCAN for the relative stability of the phases of the studied TMOs. In order to address this question, we performed calculations with the WIEN2k code to calculate the XC energy E_{XC}. We show in Figure 4 the difference $\epsilon_{XC}^{SCAN}-\epsilon_{XC}^{MGGAC}$ between the SCAN and MGGAC XC energy density [the integrand in eq 1] and in Table 3 the integral of this difference. The total E_{XC} difference

Table 3. Values (in meV/f.u.) of $E_{XC}^{SCAN} - E_{XC}^{MGGAC}$ in the *rs*-AF2 and *zb*-AF1 Phases of MnO[a]

	rs	*zb*	*rs* − *zb*
cell	5222	5031	191 (191)
Mn	2257	2215	42 (62)
O	2965	2968	−3 (−3)
interstitial	0	−152	152 (132)

[a]The results were obtained non-self-consistently (with the PBE electron density) at the SCAN equilibrium geometry using the WIEN2k code. The total values in the cell are decomposed into the Mn and O atomic spheres (of radii 1.98 and 1.71 Bohr, respectively) and interstitial. The values in parentheses in the last column were obtained with a bigger Mn atomic sphere of radius 2.10 Bohr.

in the unit cell is smaller in *zb* (5.031 eV/f.u.) as compared to *rs* (5.222 eV/f.u.), leading to a stabilization of the *rs* phase by 191 meV/f.u. with MGGAC and the correct ground state.

For a deeper analysis and to know from which spatial region this difference comes from, E_{XC} is decomposed into contributions coming from the Mn and O atomic spheres (of radii 1.98 and 1.71 Bohr, respectively), and the rest which we dub interstitial. Inside the O atomic sphere $\epsilon_{XC}^{SCAN} - \epsilon_{XC}^{MGGAC}$ is positive, indicating that the MGGAC XC energy is more negative. However, there is not much difference between the *rs* and *zb* phases, and thus also the integrals in the O atomic spheres are basically identical (only 3 meV/f.u. of difference). Inside the Mn atomic sphere there are positive (closer to the nucleus) and negative (at larger distance from the nucleus) regions of $\epsilon_{XC}^{SCAN}-\epsilon_{XC}^{MGGAC}$, but from the integrated values in Table 3 we can see that the difference is more positive in *rs* than in *zb*, leading to a slightly larger stabilization of *rs* with MGGAC relative to SCAN. $\epsilon_{XC}^{SCAN} - \epsilon_{XC}^{MGGAC}$ in the interstital region is more difficult to analyze since there are large negative (blue) regions near the atoms, but in *rs* there are also quite some positive regions far from the nuclei, which are not present in *zb*. The values in Table 3 show that $E_{XC}^{SCAN} - E_{XC}^{MGGAC}$ is virtually zero in the interstitial region of the *rs* phase (positive and negative values perfectly cancel each other) and has no effect on the stabilization, but is negative in *zb*, leading to a large destabilization of the *zb* phase with MGGAC.

This analysis can be further verified by enlarging the atomic sphere of Mn from 1.98 to 2.10 Bohr. This leads to a larger (smaller) contribution of 20 meV/f.u. coming from the Mn atomic sphere (interstitial) to the difference between the *rs* and *zb* phases of $E_{XC}^{SCAN} - E_{XC}^{MGGAC}$, as evident by the values in parentheses in Table 3. Thus, it is mainly the larger negative (blue) region around the Mn atomic sphere, where the tails of the 3*d* orbitals dominate, which produces the effect.

Figure 5 shows the difference $F_{XC}^{SCAN} - F_{XC}^{MGGAC}$ between the SCAN and MGGAC enhancement factors, where we can

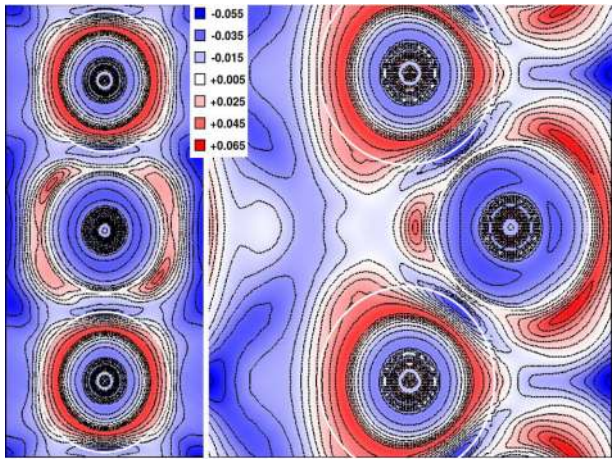

Figure 5. Two-dimensional plot in MnO of the difference $F_{XC}^{SCAN} - F_{XC}^{MGGAC}$ between the SCAN and MGGAC XC enhancement factors (see eq 1) obtained with WIEN2k from nonself-consistent calculations using the PBE electron density. The left and right panels show the (110) plane of *rs*-AF2 and the (001) plane of *zb*-AF1, respectively. The blue and red regions correspond to negative and positive values, respectively. The atoms are the same as indicated in Figure 4.

observe a similar picture (with opposite sign) as in Figure 4, namely large positive and negative differences in the atomic regions.

Since we know what is the relevant spatial region for the relative stability of the *rs*-AF2 and *zb*-AF1 phases, we can also mention the corresponding values of r_s, and of the spin-up $s_\uparrow = |\nabla n_\uparrow|/(2(6\pi^2)^{1/3} n_\uparrow^{4/3})$ and $\alpha_\uparrow^{iso} = (\tau_\uparrow - \tau_\uparrow^W)/\tau_\uparrow^{UEG}$. In the blue region of $\epsilon_{XC}^{SCAN} - \epsilon_{XC}^{MGGAC}$ around the top Mn atom in particular (the one which should have more importance since it has a full spin-up 3*d* shell) of the *zb*-AF1 phase (right panel of Figure 4), r_s is in the range 1−2 Bohr, while $s_\uparrow$ is in the range 0.5−1.0 and $\alpha_\uparrow^{iso}$ seems mostly below 1.5 (Figure 6). Then, looking at the differences between the SCAN and MGGAC enhancement factors F_{XC} (Figure 1) for the relevant values of r_s, $s_\uparrow$, and $\alpha_\uparrow^{iso}$, we can see that F_{XC}^{SCAN} should be mostly more positive than F_{XC}^{MGGAC}. Thus, since ϵ_{XC} is proportional to $-n^{4/3}F_{XC}$, then $\epsilon_{XC}^{SCAN} - \epsilon_{XC}^{MGGAC}$ (and $E_{XC}^{SCAN} - E_{XC}^{MGGAC}$) is negative in the relevant region of the *zb*-AF1 phase, leading to a stronger stabilization of the *zb*-AF1 phase when SCAN is used.

In fact, we mention again that there is a clear underestimation of the lattice constant by (r)MGGAC. This may possibly suggest that the correct energetic ordering obtained with (r)MGGAC for the different phases comes (partially) from error cancelation. However, a deeper investigation of this point is out of the scope of the present context.

CONCLUSIONS

In this work, the ability of various DFT methods to predict the correct energy ordering of the *rs* and *zb* phases of antiferromagnetic transition-metal monoxides has been studied. The case of MnO has been considered in more details. The conclusions are the following. The meta-GGAs MGGAC

https://doi.org/10.1021/acs.jpcc.2c03517
J. Phys. Chem. C 2022, 126, 14650−14660

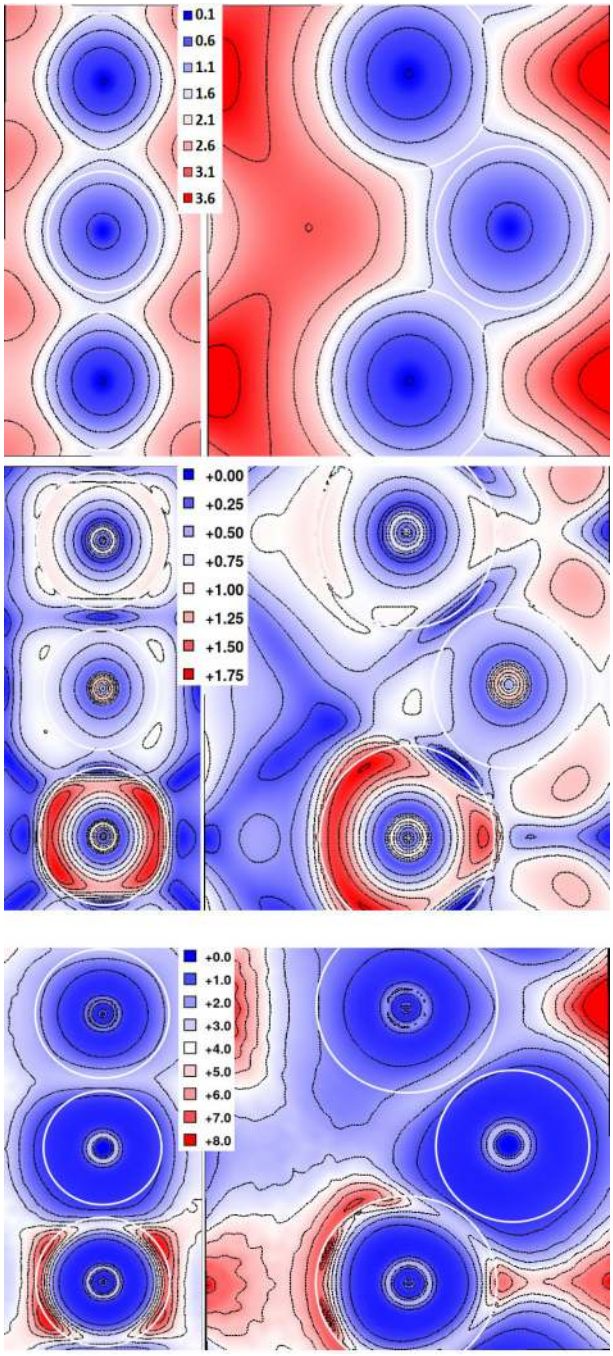

Figure 6. Two-dimensional plots in MnO of r_s (upper panels) and the spin-up reduced density gradient $s_\uparrow$ (middle panels) and iso-orbital indicator $\alpha_\uparrow^{iso}$ (lower panels), as generated using the PBE functional. The left and right panels show the (110) plane of *rs*-AF2 and the (001) plane of *zb*-AF1, respectively. The units of r_s are Bohr, while $s_\uparrow$ and $\alpha_\uparrow^{iso}$ are dimensionless. The atoms are the same as indicated in Figure 4. In both *rs*-AF2 and *zb*-AF1 panels, the top (bottom) Mn atom has a full spin-up (spin-down) 3*d* shell.

and rMGGAC provide the correct energy ordering of the *rs*-AF2 and *zb*-AF1 phases of MnO, while it is not the case with the other popular functionals PBE, SCAN, and HSE06. Furthermore, the relative energies of the two phases are in very nice agreement with the values obtained with the highly accurate DMC and RPA methods. It should be underlined that the very good (r)MGGAC results have been obtained without addition of vdW or Hubbard *U* correction. With other semilocal popular methods like PBE or SCAN, it is necessary to add a *U* or vdW correction to obtain the correct ordering of the two phases. Since also the (r)MGGAC relative energy is very accurate, this may indicate that (r)MGGAC is more accurate in the atomic regions (where, alternatively, *U* can also be added to improve the description), but also in the interstitial region (where a vdW correction may be helpful). We also showed in the present work that a relatively high amount of Hartree−Fock exchange (which plays the same role as *U*) in onsite hybrids is necessary to obtain the correct ordering of the phases of MnO.

Our results suggest that the semilocal (r)MGGAC functionals may be good alternatives to the costly DMC and RPA methods to predict the ground-state phase of strongly correlated systems. The low computational cost of semilocal methods is certainly helpful for studying potentially interesting functionalities of complex materials, such as heterostructure, cathode materials, or alloys, where various structural phases may compete.

■ ASSOCIATED CONTENT

Supporting Information

The Supporting Information is available free of charge at https://pubs.acs.org/doi/10.1021/acs.jpcc.2c03517.

Structures of all the transition metal oxides and details of the results (PDF)

■ AUTHOR INFORMATION

Corresponding Author

Subrata Jana − *Department of Chemistry and Biochemistry, The Ohio State University, Columbus, Ohio 43210, United States;* orcid.org/0000-0002-3736-1948; Email: subrata.niser@gmail.com

Authors

Arghya Ghosh − *Department of Physics, Indian Institute of Technology, Hyderabad 502285, India*

Manish K. Niranjan − *Department of Physics, Indian Institute of Technology, Hyderabad 502285, India;* orcid.org/0000-0002-4417-5107

Fabien Tran − *Institute of Materials Chemistry, Vienna University of Technology, 1060 Vienna, Austria;* orcid.org/0000-0003-4673-1987

David Wimberger − *Institute of Materials Chemistry, Vienna University of Technology, 1060 Vienna, Austria*

Peter Blaha − *Institute of Materials Chemistry, Vienna University of Technology, 1060 Vienna, Austria*

Lucian A. Constantin − *Istituto di Nanoscienze, Consiglio Nazionale delle Ricerche CNR-NANO, 41125 Modena, Italy*

Prasanjit Samal − *School of Physical Sciences, National Institute of Science Education and Research, Bhubaneswar 752050, India;* orcid.org/0000-0002-0234-8831

Complete contact information is available at: https://pubs.acs.org/10.1021/acs.jpcc.2c03517

Notes

The authors declare no competing financial interest.

■ ACKNOWLEDGMENTS

A.G. would like to thank INSPIRE fellowship, DST, India for financial support.

REFERENCES

(1) Hohenberg, P.; Kohn, W. Inhomogeneous Electron Gas. *Phys. Rev.* **1964**, *136*, B864−B871.
(2) Kohn, W.; Sham, L. J. Self-consistent equations including exchange and correlation effects. *Phys. Rev.* **1965**, *140*, A1133.
(3) Burke, K. Perspective on density functional theory. *J. Chem. Phys.* **2012**, *136*, 150901.
(4) Jones, R. O. Density functional theory: Its origins, rise to prominence, and future. *Rev. Mod. Phys.* **2015**, *87*, 897−923.
(5) Becke, A. D. Perspective: Fifty years of density-functional theory in chemical physics. *J. Chem. Phys.* **2014**, *140*, 18A301.
(6) Perdew, J. P.; Schmidt, K. Jacob's ladder of density functional approximations for the exchange-correlation energy. *AIP Conf. Proc.* **2001**, *577*, 1.
(7) Svane, A.; Gunnarsson, O. Transition-metal oxides in the self-interaction−corrected density-functional formalism. *Phys. Rev. Lett.* **1990**, *65*, 1148−1151.
(8) Peng, H.; Lany, S. Polymorphic energy ordering of MgO, ZnO, GaN, and MnO within the random phase approximation. *Phys. Rev. B* **2013**, *87*, 174113.
(9) Schrön, A.; Rödl, C.; Bechstedt, F. Energetic stability and magnetic properties of MnO in the rocksalt, wurtzite, and zinc-blende structures: Influence of exchange and correlation. *Phys. Rev. B* **2010**, *82*, 165109.
(10) Schiller, J. A.; Wagner, L. K.; Ertekin, E. Phase stability and properties of manganese oxide polymorphs: Assessment and insights from diffusion Monte Carlo. *Phys. Rev. B* **2015**, *92*, 235209.
(11) Peng, H.; Perdew, J. P. Synergy of van der Waals and self-interaction corrections in transition metal monoxides. *Phys. Rev. B* **2017**, *96*, 100101.
(12) Trimarchi, G.; Wang, Z.; Zunger, A. Polymorphous band structure model of gapping in the antiferromagnetic and paramagnetic phases of the Mott insulators MnO, FeO, CoO, and NiO. *Phys. Rev. B* **2018**, *97*, 035107.
(13) Alaei, M.; Jafari, S. Fermi surface nesting and possibility of orbital ordering in FeO. *Phys. Lett. A* **2010**, *374*, 3793−3796.
(14) Cococcioni, M.; de Gironcoli, S. Linear response approach to the calculation of the effective interaction parameters in the LDA + U method. *Phys. Rev. B* **2005**, *71*, 035105.
(15) Kanan, D. K.; Carter, E. A. Band Gap Engineering of MnO via ZnO Alloying: A Potential New Visible-Light Photocatalyst. *J. Phys. Chem. C* **2012**, *116*, 9876−9887.
(16) Toroker, M. C.; Carter, E. A. Transition metal oxide alloys as potential solar energy conversion materials. *J. Mater. Chem. A* **2013**, *1*, 2474−2484.
(17) Peng, H.; Lany, S. Semiconducting transition-metal oxides based on d^5 cations: Theory for MnO and Fe_2O_3. *Phys. Rev. B* **2012**, *85*, 201202.
(18) Gopal, P.; Spaldin, N. A.; Waghmare, U. V. First-principles study of wurtzite-structure MnO. *Phys. Rev. B* **2004**, *70*, 205104.
(19) Archer, T.; Pemmaraju, C. D.; Sanvito, S.; Franchini, C.; He, J.; Filippetti, A.; Delugas, P.; Puggioni, D.; Fiorentini, V.; Tiwari, R.; Majumdar, P. Exchange interactions and magnetic phases of transition metal oxides: Benchmarking advanced ab initio methods. *Phys. Rev. B* **2011**, *84*, 115114.
(20) Franchini, C.; Bayer, V.; Podloucky, R.; Paier, J.; Kresse, G. Density functional theory study of MnO by a hybrid functional approach. *Phys. Rev. B* **2005**, *72*, 045132.
(21) Roth, W. L. Magnetic Structures of MnO, FeO, CoO, and NiO. *Phys. Rev.* **1958**, *110*, 1333−1341.
(22) Jana, S.; Constantin, L. A.; Śmiga, S.; Samal, P. Solid-state performance of a meta-GGA screened hybrid density functional constructed from Pauli kinetic enhancement factor dependent semilocal exchange hole. *J. Chem. Phys.* **2022**, *157*, 024102.
(23) Zhang, Y.; Furness, J.; Zhang, R.; Wang, Z.; Zunger, A.; Sun, J. Symmetry-breaking polymorphous descriptions for correlated materials without interelectronic U. *Phys. Rev. B* **2020**, *102*, 045112.
(24) Sai Gautam, G.; Carter, E. A. Evaluating transition metal oxides within DFT-SCAN and SCAN + *U* frameworks for solar thermochemical applications. *Phys. Rev. Materials* **2018**, *2*, 095401.
(25) Tran, F.; Ehsan, S.; Blaha, P. Assessment of the GLLB-SC potential for solid-state properties and attempts for improvement. *Phys. Rev. Materials* **2018**, *2*, 023802.
(26) Tran, F.; Baudesson, G.; Carrete, J.; Madsen, G. K. H.; Blaha, P.; Schwarz, K.; Singh, D. J. Shortcomings of meta-GGA functionals when describing magnetism. *Phys. Rev. B* **2020**, *102*, 024407.
(27) Anisimov, V. I.; Zaanen, J.; Andersen, O. K. Band theory and Mott insulators: Hubbard U instead of Stoner I. *Phys. Rev. B* **1991**, *44*, 943−954.
(28) Schrön, A.; Rödl, C.; Bechstedt, F. Crystalline and magnetic anisotropy of the 3*d*-transition metal monoxides MnO, FeO, CoO, and NiO. *Phys. Rev. B* **2012**, *86*, 115134.
(29) Tran, F.; Blaha, P.; Schwarz, K.; Novák, P. Hybrid Exchange-Correlation Energy Functionals for Strongly Correlated Electrons: Applications to Transition-Metal Monoxides. *Phys. Rev. B* **2006**, *74*, 155108.
(30) Marsman, M.; Paier, J.; Stroppa, A.; Kresse, G. Hybrid functionals applied to extended systems. *J. Phys.: Condens. Matter* **2008**, *20*, 064201.
(31) Liu, P.; Franchini, C.; Marsman, M.; Kresse, G. Assessing model-dielectric-dependent hybrid functionals on the antiferromagnetic transition-metal monoxides MnO, FeO, CoO, and NiO. *J. Phys.: Condens. Matter* **2019**, *32*, 015502.
(32) Jana, S.; Patra, A.; Samal, P. Efficient lattice constants and energy bandgaps for condensed systems from a meta-GGA level screened range-separated hybrid functional. *J. Chem. Phys.* **2018**, *149*, 094105.
(33) Jana, S.; Samal, P. Screened hybrid meta-GGA exchange-correlation functionals for extended systems. *Phys. Chem. Chem. Phys.* **2019**, *21*, 3002−3015.
(34) Jana, S.; Patra, A.; Constantin, L. A.; Samal, P. Screened range-separated hybrid by balancing the compact and slowly varying density regimes: Satisfaction of local density linear response. *J. Chem. Phys.* **2020**, *152*, 044111.
(35) Jana, S.; Patra, B.; Śmiga, S.; Constantin, L. A.; Samal, P. Improved solid stability from a screened range-separated hybrid functional by satisfying semiclassical atom theory and local density linear response. *Phys. Rev. B* **2020**, *102*, 155107.
(36) Solovyev, I. V.; Terakura, K. Effective single-particle potentials for MnO in light of interatomic magnetic interactions: Existing theories and perspectives. *Phys. Rev. B* **1998**, *58*, 15496−15507.
(37) Engel, E.; Schmid, R. N. Insulating Ground States of Transition-Metal Monoxides from Exact Exchange. *Phys. Rev. Lett.* **2009**, *103*, 036404.
(38) Erten, O.; Meetei, O. N.; Mukherjee, A.; Randeria, M.; Trivedi, N.; Woodward, P. Theory of Half-Metallic Ferrimagnetism in Double Perovskites. *Phys. Rev. Lett.* **2011**, *107*, 257201.
(39) Hossain, M.; De, J.; Bhattacharjee, J. Hybrid Atomic Orbital Basis from First Principles: Bottom-Up Mapping of Self-Energy Correction to Large Covalent Systems. *J. Phys. Chem. A* **2021**, *125*, 6805−6817.
(40) Hossain, M.; Bhattacharjee, J. Transferability of self-energy correction in tight-binding basis constructed from first principles. *J. Chem. Phys.* **2020**, *153*, 144103.
(41) Massidda, S.; Continenza, A.; Posternak, M.; Baldereschi, A. Quasiparticle energy bands of transition-metal oxides within a model GW scheme. *Phys. Rev. B* **1997**, *55*, 13494−13502.
(42) Kotani, T.; van Schilfgaarde, M. Spin wave dispersion based on the quasiparticle self-consistent *GW* method: NiO, MnO and *α*-MnAs. *J. Phys.: Condens. Matter* **2008**, *20*, 295214.
(43) Rödl, C.; Fuchs, F.; Furthmüller, J.; Bechstedt, F. Quasiparticle band structures of the antiferromagnetic transition-metal oxides MnO, FeO, CoO, and NiO. *Phys. Rev. B* **2009**, *79*, 235114.
(44) Kuneš, J.; Lukoyanov, A.; Anisimov, V.; Scalettar, R. T.; Pickett, W. E. Collapse of magnetic moment drives the Mott transition in MnO. *Nat. Mater.* **2008**, *7*, 198−202.

https://doi.org/10.1021/acs.jpcc.2c03517
J. Phys. Chem. C 2022, 126, 14650−14660

(45) Mandal, S.; Haule, K.; Rabe, K. M.; Vanderbilt, D. Systematic beyond-DFT study of binary transition metal oxides. *npj Computational Materials* **2019**, *5*, 115.
(46) Mukherjee, A.; Patel, N. D.; Dong, S.; Johnston, S.; Moreo, A.; Dagotto, E. Testing the Monte Carlo−mean field approximation in the one-band Hubbard model. *Phys. Rev. B* **2014**, *90*, 205133.
(47) Sun, J.; Ruzsinszky, A.; Perdew, J. P. Strongly constrained and appropriately normed semilocal density functional. *Phys. Rev. Lett.* **2015**, *115*, 036402.
(48) Sabatini, R.; Gorni, T.; de Gironcoli, S. Nonlocal van der Waals density functional made simple and efficient. *Phys. Rev. B* **2013**, *87*, No. 041108.
(49) Jana, S.; Patra, A.; Samal, P. Assessing the performance of the Tao-Mo semilocal density functional in the projector-augmented-wave method. *J. Chem. Phys.* **2018**, *149*, 044120.
(50) Patra, A.; Jana, S.; Samal, P. A way of resolving the order-of-limit problem of Tao−Mo semilocal functional. *J. Chem. Phys.* **2020**, *153*, 184112.
(51) Jana, S.; Behera, S. K.; Śmiga, S.; Constantin, L. A.; Samal, P. Accurate density functional made more versatile. *J. Chem. Phys.* **2021**, *155*, 024103.
(52) Jana, S.; Constantin, L. A.; Samal, P. Accurate Water Properties from an Efficient ab Initio Method. *J. Chem. Theory Comput.* **2020**, *16*, 974−987.
(53) Jana, S.; Patra, A.; Śmiga, S.; Constantin, L. A.; Samal, P. Insights from the density functional performance of water and water-solid interactions: SCAN in relation to other meta-GGAs. *J. Chem. Phys.* **2020**, *153*, 214116.
(54) Ghosh, A.; Jana, S.; Niranjan, M.; Behera, S. K.; Constantin, L. A.; Samal, P. Improved electronic structure prediction of chalcopyrite semiconductors from a semilocal density functional based on Pauli kinetic energy enhancement factor. *J. Phys.: Condens. Matter* **2021**, na.
(55) Tran, F.; Stelzl, J.; Blaha, P. Rungs 1 to 4 of DFT Jacob's ladder: Extensive test on the lattice constant, bulk modulus, and cohesive energy of solids. *J. Chem. Phys.* **2016**, *144*, 204120.
(56) Sengupta, N.; Bates, J. E.; Ruzsinszky, A. From semilocal density functionals to random phase approximation renormalized perturbation theory: A methodological assessment of structural phase transitions. *Phys. Rev. B* **2018**, *97*, 235136.
(57) Shahi, C.; Sun, J.; Perdew, J. P. Accurate critical pressures for structural phase transitions of group IV, III-V, and II-VI compounds from the SCAN density functional. *Phys. Rev. B* **2018**, *97*, 094111.
(58) Peng, H.; Yang, Z.-H.; Perdew, J. P.; Sun, J. Versatile van der Waals Density Functional Based on a Meta-Generalized Gradient Approximation. *Phys. Rev. X* **2016**, *6*, 041005.
(59) Mo, Y.; Car, R.; Staroverov, V. N.; Scuseria, G. E.; Tao, J. Assessment of the Tao-Mo nonempirical semilocal density functional in applications to solids and surfaces. *Phys. Rev. B* **2017**, *95*, 035118.
(60) Jana, S.; Sharma, K.; Samal, P. Assessing the performance of the recent meta-GGA density functionals for describing the lattice constants, bulk moduli, and cohesive energies of alkali, alkaline-earth, and transition metals. *J. Chem. Phys.* **2018**, *149*, 164703.
(61) Jana, S.; Sharma, K.; Samal, P. Improving the Performance of Tao−Mo Non-empirical Density Functional with Broader Applicability in Quantum Chemistry and Materials Science. *J. Phys. Chem. A* **2019**, *123*, 6356−6369.
(62) Patra, B.; Jana, S.; Constantin, L. A.; Samal, P. Relevance of the Pauli kinetic energy density for semilocal functionals. *Phys. Rev. B* **2019**, *100*, 155140.
(63) Patra, A.; Jana, S.; Samal, P. Performance of Tao-Mo Semilocal Functional with rVV10 Dispersion-Correction: Influence of Different Correlation. *J. Phys. Chem. A* **2019**, *123*, 10582−10593.
(64) Patra, B.; Jana, S.; Constantin, L. A.; Samal, P. Correct Structural Phase Stability of FeS2, TiO2, and MnO2 from a Semilocal Density Functional. *J. Phys. Chem. C* **2021**, *125*, 4284−4291.
(65) Jana, S.; Behera, S. K.; Śmiga, S.; Constantin, L. A.; Samal, P. Improving the applicability of the Pauli kinetic energy density based semilocal functional for solids. *New J. Phys.* **2021**, *23*, 063007.
(66) Patra, A.; Patra, B.; Constantin, L. A.; Samal, P. Electronic band structure of layers within meta generalized gradient approximation of density functionals. *Phys. Rev. B* **2020**, *102*, 045135.
(67) Patra, A.; Jana, S.; Samal, P.; Tran, F.; Kalantari, L.; Doumont, J.; Blaha, P. Efficient Band Structure Calculation of Two-Dimensional Materials from Semilocal Density Functionals. *J. Phys. Chem. C* **2021**, *125*, 11206−11215.
(68) Tran, F.; Doumont, J.; Kalantari, L.; Blaha, P.; Rauch, T.; Borlido, P.; Botti, S.; Marques, M. A. L.; Patra, A.; Jana, S.; Samal, P. Bandgap of two-dimensional materials: Thorough assessment of modern exchange−correlation functionals. *J. Chem. Phys.* **2021**, *155*, 104103.
(69) Novák, P.; Kuneš, J.; Chaput, L.; Pickett, W. E. Exact exchange for correlated electrons. *physica status solidi (b)* **2006**, *243*, 563−572.
(70) Perdew, J. P.; Burke, K.; Ernzerhof, M. Generalized gradient approximation made simple. *Phys. Rev. Lett.* **1996**, *77*, 3865.
(71) Furness, J. W.; Kaplan, A. D.; Ning, J.; Perdew, J. P.; Sun, J. Accurate and Numerically Efficient r2SCAN Meta-Generalized Gradient Approximation. *J. Phys. Chem. Lett.* **2020**, *11*, 8208−8215.
(72) Sun, J.; Xiao, B.; Fang, Y.; Haunschild, R.; Hao, P.; Ruzsinszky, A.; Csonka, G. I.; Scuseria, G. E.; Perdew, J. P. Density Functionals that Recognize Covalent, Metallic, and Weak Bonds. *Phys. Rev. Lett.* **2013**, *111*, 106401.
(73) Della Sala, F.; Fabiano, E.; Constantin, L. A. Kinetic-energy-density dependent semilocal exchange-correlation functionals. *Int. J. Quantum Chem.* **2016**, *116*, 1641−1694.
(74) Furness, J. W.; Sengupta, N.; Ning, J.; Ruzsinszky, A.; Sun, J. Examining the order-of-limits problem and lattice constant performance of the Tao−Mo functional. *J. Chem. Phys.* **2020**, *152*, 244112.
(75) Tao, J.; Perdew, J. P.; Staroverov, V. N.; Scuseria, G. E. Climbing the Density Functional Ladder: Nonempirical Meta−Generalized Gradient Approximation Designed for Molecules and Solids. *Phys. Rev. Lett.* **2003**, *91*, 146401.
(76) Tao, J.; Mo, Y. Accurate semilocal density functional for condensed-matter physics and quantum chemistry. *Phys. Rev. Lett.* **2016**, *117*, 073001.
(77) Ruzsinszky, A.; Sun, J.; Xiao, B.; Csonka, G. I. A meta-GGA Made Free of the Order of Limits Anomaly. *J. Chem. Theory Comput.* **2012**, *8*, 2078−2087.
(78) Becke, A. D.; Roussel, M. R. Exchange holes in inhomogeneous systems: A coordinate-space model. *Phys. Rev. A* **1989**, *39*, 3761−3767.
(79) Patra, B.; Jana, S.; Constantin, L. A.; Samal, P. Efficient band gap prediction of semiconductors and insulators from a semilocal exchange-correlation functional. *Phys. Rev. B* **2019**, *100*, 045147.
(80) Perdew, J. P.; Ruzsinszky, A.; Sun, J.; Burke, K. Gedanken densities and exact constraints in density functional theory. *J. Chem. Phys.* **2014**, *140*, 18A533.
(81) Aschebrock, T.; Kümmel, S. Ultranonlocality and accurate band gaps from a meta-generalized gradient approximation. *Phys. Rev. Res.* **2019**, *1*, 033082.
(82) Kresse, G.; Hafner, J. Ab initio molecular dynamics for liquid metals. *Phys. Rev. B* **1993**, *47*, 558−561.
(83) Kresse, G.; Furthmüller, J. Efficient iterative schemes for ab initio total-energy calculations using a plane-wave basis set. *Phys. Rev. B* **1996**, *54*, 11169−11186.
(84) Kresse, G.; Furthmüller, J. Efficiency of ab-initio total energy calculations for metals and semiconductors using a plane-wave basis set. *Comput. Mater. Sci.* **1996**, *6*, 15−50.
(85) Kresse, G.; Joubert, D. From ultrasoft pseudopotentials to the projector augmented-wave method. *Phys. Rev. B* **1999**, *59*, 1758−1775.
(86) Blöchl, P. E. Projector augmented-wave method. *Phys. Rev. B* **1994**, *50*, 17953−17979.
(87) Blaha, P.; Schwarz, K.; Madsen, G. K. H.; Kvasnicka, D.; Luitz, J.; Laskowski, R.; Tran, F.; Marks, L. D. *WIEN2k: An Augmented Plane Wave plus Local Orbitals Program for Calculating Crystal Properties*; Vienna University of Technology: Austria, 2018.

https://doi.org/10.1021/acs.jpcc.2c03517
J. Phys. Chem. C 2022, 126, 14650−14660

(88) Blaha, P.; Schwarz, K.; Tran, F.; Laskowski, R.; Madsen, G. K. H.; Marks, L. D. WIEN2k: An APW+lo program for calculating the properties of solids. *J. Chem. Phys.* **2020**, *152*, 074101.
(89) Singh, D. J.; Nordström, L. *Planewaves, Pseudopotentials, and the LAPW Method*, 2nd ed.; Springer: New York, 2006.
(90) Karsai, F.; Tran, F.; Blaha, P. On the importance of local orbitals using second energy derivatives for d and f electrons. *Comput. Phys. Commun.* **2017**, *220*, 230−238.
(91) See http://link.aps.org/supplemental/ for a detailed description of the considered phases and numerical results.
(92) Birch, F. Finite Elastic Strain of Cubic Crystals. *Phys. Rev.* **1947**, *71*, 809−824.
(93) Tkatchenko, A.; Scheffler, M. Accurate Molecular Van Der Waals Interactions from Ground-State Electron Density and Free-Atom Reference Data. *Phys. Rev. Lett.* **2009**, *102*, 073005.
(94) Vydrov, O. A.; Van Voorhis, T. Nonlocal van der Waals density functional: The simpler the better. *J. Chem. Phys.* **2010**, *133*, 244103.
(95) Roth, W. L. Magnetic Structures of MnO, FeO, CoO, and NiO. *Phys. Rev.* **1958**, *110*, 1333−1341.
(96) Cheetham, A. K.; Hope, D. A. O. Magnetic ordering and exchange effects in the antiferromagnetic solid solutions $Mn_xNi_{1-x}O$. *Phys. Rev. B* **1983**, *27*, 6964−6967.
(97) Shaked, H.; Faber, J.; Hitterman, R. L. low-temperature magnetic structure of mno: a high-resolution neutron-diffraction study. *Phys. Rev. B* **1988**, *38*, 11901−11903.
(98) Webb, S.; Jackson, I.; Fitz Gerald, J. High-pressure elasticity, shear-mode softening and polymorphism in MnO. *Physics of the Earth and Planetary Interiors* **1988**, *52*, 117−131.
(99) Pacalo, R. E.; Graham, E. K. Pressure and temperature dependence of the elastic properties of synthetic MnO. *Physics and Chemistry of Minerals* **1991**, *18*, 69−80.
(100) Zhang, J. Room-temperature compressibilities of MnO and CdO: further examination of the role of cation type in bulk modulus systematics. *Physics and Chemistry of Minerals* **1999**, *26*, 644−648.
(101) Kim, M.-C.; Sim, E.; Burke, K. Understanding and Reducing Errors in Density Functional Calculations. *Phys. Rev. Lett.* **2013**, *111*, 073003.
(102) Kuisma, M.; Ojanen, J.; Enkovaara, J.; Rantala, T. T. Kohn-Sham Potential with Discontinuity for Band Gap Materials. *Phys. Rev. B* **2010**, *82*, 115106.
(103) Finzel, K.; Baranov, A. I. A Simple Model for the Slater Exchange Potential and its Performance for Solids. *Int. J. Quantum Chem.* **2017**, *117*, 40−47.
(104) Bader, R. F. W. *Atoms in Molecules: A Quantum Theory*; Oxford University Press: Oxford, 1990.
(105) Bader, R. F. W. A quantum theory of molecular structure and its applications. *Chem. Rev.* **1991**, *91*, 893−928.
(106) Hamada, I. van der Waals density functional made accurate. *Phys. Rev. B* **2014**, *89*, 121103.
(107) Saritas, K.; Krogel, J. T.; Reboredo, F. A. Relative energies and electronic structures of CoO polymorphs through ab initio diffusion quantum Monte Carlo. *Phys. Rev. B* **2018**, *98*, 155130.
(108) Boyle, B. J.; King, E. G.; Conway, K. C. Heats of Formation of Nickel and Cobalt Oxides (NiO and CoO) of Combustion Calorimetry. *J. Am. Chem. Soc.* **1954**, *76*, 3835−3837.

https://doi.org/10.1021/acs.jpcc.2c03517
J. Phys. Chem. C 2022, 126, 14650−14660